Contents lists available at **CEPM**

Computational Engineering and Physical Modeling

Journal homepage: www.jcepm.com

Fragility of a Weir Structure due to Scouring

S. S. Bodda[1*], A. Gupta[1], B. S. Ju[2], W. Y. Jung[3]

1. Center for Nuclear Energy Facilities and Structures, CCEE, North Carolina State University, Raleigh, NC, USA
2. Department of Civil Engineering, KyungHee University, Gyeonggi-do, Republic of Korea
3. Institute for Disaster Prevention, Gangneung-Wonju National University, Gangneung 210-702, Republic of Korea

Corresponding author: *ssbodda@ncsu.edu*

https://doi.org/10.22115/CEPM .2020.214539.1077

ARTICLE INFO

Article history:
Received: 04 January 2020
Revised: 03 March 2020
Accepted: 08 March 2020

Keywords:
Flooding;
Seepage analysis;
Finite element model;
Probabilistic risk assessment.

ABSTRACT

In recent years, several catastrophic flooding accidents have occurred at critical facilities. The Arkema chemical plant in Texas suffered chemical explosion because hurricane Harvey related flooding resulted in a loss of power supply. Fukushima Daiichi nuclear disaster occurred due to loss of external and backup power supplies following the tsunami induced flooding. In order to prevent flooding at such critical and toxic facilities, flood protection systems such as weir structures or floodwalls are being planned or have been constructed. The risk of flooding at critical facilities which are located on the downstream side of a flood defense structure is directly related to the fragility of flood defense structure. All the flood defense structures are subjected to scour around their foundations. The stability of the foundation is endangered when the scour depth becomes significant at the downstream toe. This paper explores the effect of scouring on the fragility of a concrete weir structure.

1. Introduction

According to FEMA [1], 20 dams were breached due to foundation failures, flood overflow, and concrete cracks as a result of flooding due to Hurricane Matthew in North Carolina. Flooding

How to cite this article: Bodda SS, Gupta A, Ju BS, Jung W. Fragility of a Weir Structure due to Scouring. Comput Eng Phys Model 2020;3:1–15. https://doi.org/10.22115/cepm.2020.214539.1077.

produced by Hurricane Katrina breached many levees which resulted in flooding of approximately 75% of the New Orleans metropolitan area [2].

The data for generating the flooding fragility curves for foundation failure is obtained from a seepage analysis. Therefore, the reliability of the fragility curves largely depends on accuracy of the seepage model. Various methods such as flow nets, experimental and numerical methods (finite difference and finite elements) have been used in the past to solve the two-dimensional partial differential equation for seepage flow [3–8]. USACE [3] uses graphical flow nets for estimating seepage through embankments and foundations. Numerical modeling has been used successfully to solve seepage problems [9]. Billstein *et al*. [4] use numerical, analytical and experimental models to determine the seepage levels and discharge. Saleh [5] uses FE modeling to analyze seepage flow under weir foundation. Kolawole [6] and Kirra *et al*. [7] use FE modeling to study seepage through earth dams. Bardet[10] uses finite difference methods for solving free surface seepage problems. Finite element method is widely preferred because of its ability to handle complex geometries (and boundaries) with relative ease.

Flood defense structures are subjected to scour around their foundations. If the scour depth becomes significant, the foundation of the structure is exposed, with a consequent risk of failure due to rupture. Therefore, it is important to study the effect of scour on foundation failure. Failures of Woodlake dam[1] and Hope Mills dam occurred primarily due to scouring. While several studies have been conducted in the past to evaluate the effect of seepage [5–8,11] , none of these studies consider the effect of scouring, which is typically the primary initiator of the foundation failure. In this paper, we present the results of a study that evaluates the effect of scouring on the fragility of concrete weir structure. Given the uncertainties in the soil properties as well as the potential erosion profiles, a probabilistic study is conducted by considering uncertainties in relevant properties to evaluate the fragility curves (probabilities of failure). Variation in these curves due to a change in scour profile is also presented. To begin with, a finite element based approach appeared to be straightforward for conducting this study. However, it exhibited challenges associated with computational efficiency, numerical stability, and accuracy. These challenges and the solutions to overcome them are also presented in this paper. The significance of these findings might appear simple but are critical in the context of many recent articles that have proposed the development of artificial neural networks and other data-driven approaches for fragility assessment of such structures. Such data-driven approaches rely on using extensive data from large scale finite element simulations and can give incorrect predictions if incorrect and non-convergent finite element models are used for generating the data.

2. Problem description

As mentioned above, a primary reason for failure of flood defense structures is related to seepage through the soil which has the potential to cause internal erosion and scouring on the downstream of the structure. Even at low hydraulic heads, the flow over a structure such as weir has a significant potential for scouring. Hence, stilling basins are placed at the ends of weir spillways to dissipate the energy of water exiting the spillway and mitigate scouring. However, local scour downstream of stilling basins is considered as an important phenomenon as it can

endanger the stability of the foundation with a consequent risk of failure when the scour depth becomes significant [12]. The study presented in this paper is carried out for a simple model of weir structure. However, the concepts are directly applicable to any concrete flood defense structure.

2.1. Description of the weir structure

Geometry and dimensions of the particular section of a weir structure foundation considered for this study are shown in Fig. 1 [13]. Potential head on upstream is $H_{u/s} = 11\,m$. The soil foundation at the site consists of silty sand. A part of the weir's concrete structure is built into the foundation with a depth of 10 m. To begin with, the width (B) and depth (D) of the elastic half space are assumed to be $B = 80\,m$ and $D = 50\,m$ respectively. These dimensions are consistent with the values considered in many prior studies [5–8]. B_1 and B_2 are the widths of the soil domain on upstream side and downstream side of the weir structure, respectively.

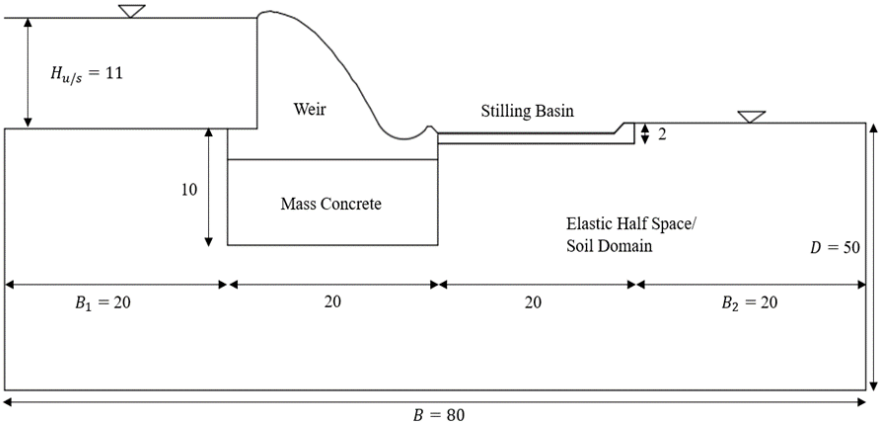

Fig. 1. Geometry and Dimensions (m) of the Weir structure foundation [13].

2.2. Steady-state seepage formulation

All flood defense structures have some seepage (flow of water through soils) as there is difference in water pressure between upstream and downstream sides of the defense structure. Seepage of water through foundation depends on several factors, including the soil permeability, hydraulic gradient, and type of flow. Higher water levels in the reservoir results in higher gradient for seepage through the foundation and thereby increasing the subsequent chances of the foundation failure. Uncontrolled seepage can slowly erode soil from flood defense structure's foundation. Erosion of the soil starts at the downstream side of the flood defense structure and advances progressively toward the reservoir, creating a hollow pipe like formation to the reservoir, leading to foundation failure and hence, collapse of the structure. This phenomenon is known as piping or undermining.

The two-dimensional steady-state flow of the pore fluid is governed by Laplace's equation, as shown in Eq. (1):

$$K_x \frac{d^2H}{dx^2} + K_y \frac{d^2H}{dy^2} = 0 \tag{1}$$

where: K_x and K_y are the hydraulic conductivity in the x and y directions respectively and H is the hydraulic head.

The seepage flow q_x and q_y in the x and y directions respectively is calculated from Darcy's law as shown in Eq. (2). These flow quantities are directed either in the x direction or in the y direction. The total flow at any point in the foundation is the resultant of the q_x and q_y at that point. Thus, the total seepage-flow vector is directed so that it is perpendicular to the lines of constant head (equipotential lines) in the foundation, as shown in Fig. 2.

$$q_x = -K_x \frac{\partial H}{\partial x}$$

$$q_y = -K_y \frac{\partial H}{\partial y} \tag{2}$$

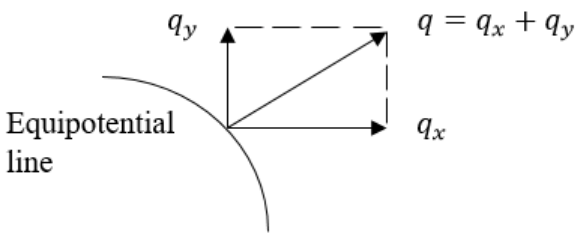

Fig. 2. Fluid flow in two directions.

The Galerkin's discretization of the Laplace equation gives the following relation:

$$[K]\{H\} = \{Q\} \tag{3}$$

where: $[K]$ is the global stiffness matrix, $\{H\}$ is an unknown nodal total head vector, and $\{Q\}$ is a nodal flow vector.

The global stiffness matrix $[K]$ is an assembly of the element stiffness matrices of the entire flow domain. The element stiffness matrix is given as:

$$[K] = \int_{v_e} [B]^T [k][B] dv \tag{4}$$

where: v_e is the domain of the element, $[B]$ is derived from the shape function $[N]$, and $[k]$ is the element permeability matrix, defined as

$$[k] = \begin{bmatrix} K_x & 0 \\ 0 & K_y \end{bmatrix} \tag{5}$$

In this study, the seepage equation is solved using FE method based on the approach by Kratochvil [14] and Kirra [7].

2.3. Performance criterion

A fragility assessment requires characterization of failure in terms of a performance function. The performance function defines the governing limit-state to evaluate the probabilities of failure. In this study, the performance function characterizes failure as a rupture of the

foundation. Rupture of the foundation occurs when maximum exit gradient exceeds the critical gradient [8,15]. The exit gradient (i_{ex}) is the total head loss divided by distance of flow between the two measured head locations, calculated at the downstream area where seepage exits the porous media. The area of significance in this study is along the downstream edge of weir structure for confined flow. The exit gradient is calculated along the downstream side, and maximum gradient usually occurs near the toe of the stilling basin. Also, for a two-dimensional model, the exit gradient depends upon the gradient direction. The critical gradient (i_{cr}) is based on the foundation soil properties.

$$i_{cr} = (G_s - 1)(1 - n) \tag{6}$$

$$i_{ex} = \frac{dH}{dL} \tag{7}$$

where: n is the porosity of the soil, and G_s is the specific gravity of the soil.

The performance function for rupture is characterized by following limit state:

$$Z_r = i_{cr} - i_{ex} \tag{8}$$

And the conditional probability of failure due to rupture given flood height is expressed as:

$$P_f(rupture|flood\ height) = P(Z_r < 0) \tag{9}$$

For the worst case scenario of the rupture to occur, minimum value of specific gravity and maximum value of porosity are chosen from various ranges of soil specific gravity and porosity so that the hydraulic critical gradient is minimum [8]. The minimum critical gradient calculated for three different types of soils (Eq. 6) is shown in Table 1.

Table 1. Minimum critical gradient for sand, silt, and clay soils.

	Soil Type	**Specific Gravity**	**Porosity (%)**	**Minimum Critical Gradient (i_{cr})**
1	Sand	2.63	53	0.7661
2	Silt	2.65	61	0.6435
3	Clay	2.70	57	0.7310

3. Finite element modeling

3.1 Efficiency

A probabilistic study to evaluate fragilities requires a large number of finite element analyses. Therefore, computational efficiency is an important consideration. The type and the size of specific elements used for creating the model can have a significant impact on both the efficiency as well as accuracy. In most of the prior studies [5–7,11,16], 4-noded quadratic elements are used to model the seepage problem. In this study, we observe that this element type requires a very fine mesh in order to accurately model the scour profile which in turn makes the analysis

computationally inefficient. Therefore, alternative element types are explored. Two types of alternatives considered include the use of a 6-noded triangular element and an 8-noded quadratic element. These two element types are chosen because of their ability to represent curved scour profiles accurately through a relatively coarser mesh. In order to compare the efficiency and accuracy of these different element types, a simpler case with no scouring is considered. The effect of scouring is studied after a particular element type is selected.

The two-dimensional finite element idealization of the foundation consists of uniform elements with an element size of 'h' meters in both the horizontal and vertical directions. The soil layer is assumed to be homogenous and isotropic with respect to permeability. Fig. 3. shows the results of the convergence (accuracy) as well as computational efficiency conducted for the 3 types of elements considered. Computation time 't' is taken as the unit time equal to the run time of the FE model with 4-noded elements of an element size $h = 2\,m$. The computation time for other mesh sizes and elements are expressed as a multiple of t.

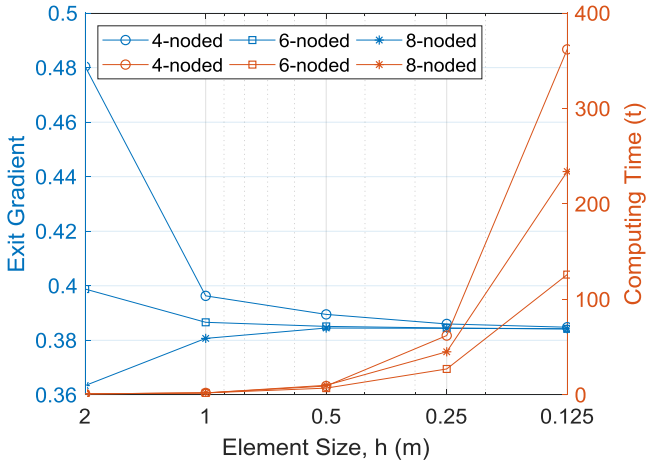

Fig 3. Results of convergence study.

According to the convergence analysis, quadratic elements (8-noded and 6-noded) exhibits much smaller error than linear elements (4-noded) for the same element size, which is expected due to richer interpolation in 8-noded and 6-noded elements. Based on optimal combination of accuracy and efficiency, the FE model with 8-noded elements of $h = 0.5\,m$ is chosen for the further analysis.

3.2. Numerical ınstability

A seepage analysis provides information of flow magnitude and the direction of flow in different regions of the foundation. Such a spatial mapping of the flow is represented in terms of hydraulic gradient vectors. Selection of element size not only influences convergence and computational efficiency as discussed in the previous section, it can also cause numerical instability particularly in the evaluation of hydraulic exit gradient. To illustrate this, let us consider the plot of gradient vectors shown in Fig. 4. The gradient vectors in this figure are evaluated for the case of an element size $h = 2\,m$ and the point B represents the toe, i.e. the thickness of stilling basin is equal to the element size. It can be observed that the maximum exit gradient occurs at surface of

the toe of stilling basin. In this particular case, the exit gradient is calculated based on Eq. (10), in which the hydraulic head at point B is also the hydraulic head at toe ($H_B = H_{toe}$).

$$i_{ex} = \frac{H_A - H_B}{L_{AB}} \tag{10}$$

However, the toe is a sharp reentrant corner which is a point of discontinuity in the foundation profile. The discontinuity would therefore result in a singularity, i.e. the derivatives of the dependent variables for partial differential equation (Eq. 1) do not exist at the sharp toe thereby resulting in a numerical instability.

A smaller element size allows more than one element to span across the thickness of the stilling basin and the point B moves away from the toe. For example, in the case of $h = 0.5\ m$, the exit gradient is not influenced by the sharp corner at the toe. The gradient vectors near the toe of the stilling basin for $h = 0.5\ m$ are shown in Fig. 5.

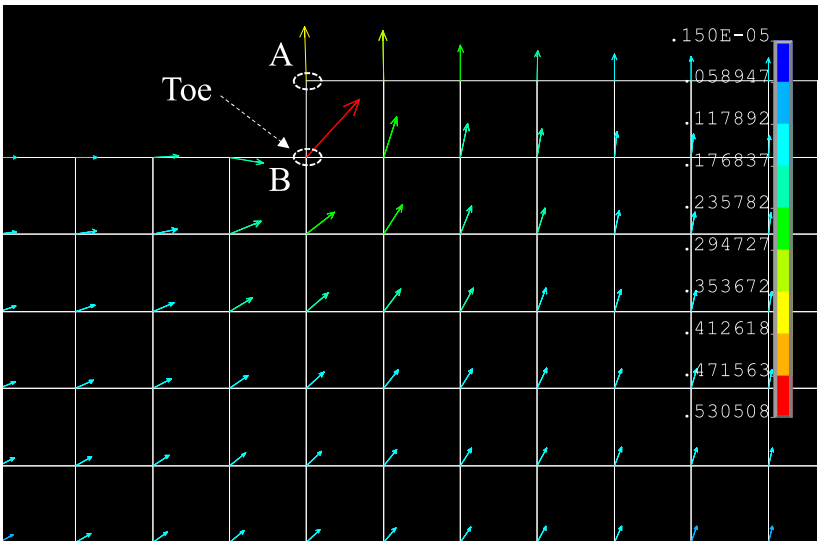

Fig. 4. Vector plot of hydraulic gradient using 8-noded element of size $h = 2\ m$.

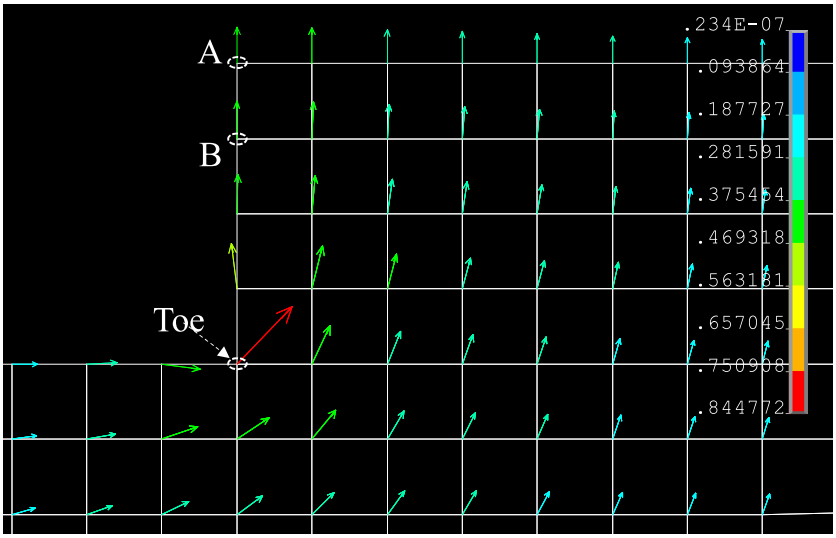

Fig. 5. Vector plot of hydraulic gradient using 8-noded element of size $h = 0.5\ m$.

3.3. Convergence and accuracy

In general, the soil domain is considered as a semi-infinite or an elastic half space, i.e. a finite soil domain is modelled such that there is no effect of limited domain on the exit gradient. The dimensions of various flood defense structures considered for the seepage analysis are mentioned in previous studies [5,11,17,18], but none of these studies have given any guidance on the size of the elastic half space. The size of the elastic half space can make a significant difference in exit gradient calculation as seen in Fig. 6. If the upstream width and depth of the soil domain is less than an optimal size, then the results are underestimated and if the downstream width of the soil domain is less than an optimal size, then the results are overestimated.

The optimal dimensions of the soil domain are assessed through a convergence study on maximum exit gradient as shown in Fig. 6. This study comprised of following three steps.

Step 1: The upstream (U/S) width is calculated by fixing both the downstream (D/S) width and depth of the soil domain.

Step 2: The D/S width is calculated by fixing the depth of the soil domain, and the U/S width obtained from step 1.

Step 3: The depth of the soil domain is calculated by fixing the U/S and D/S widths obtained from step 1 and step 2.

It is observed that the upstream width (B_1), the downstream width (B_2), and the depth (D) of the elastic half space should be at least two and half times more than the combined width of the weir structure and the stilling basin.

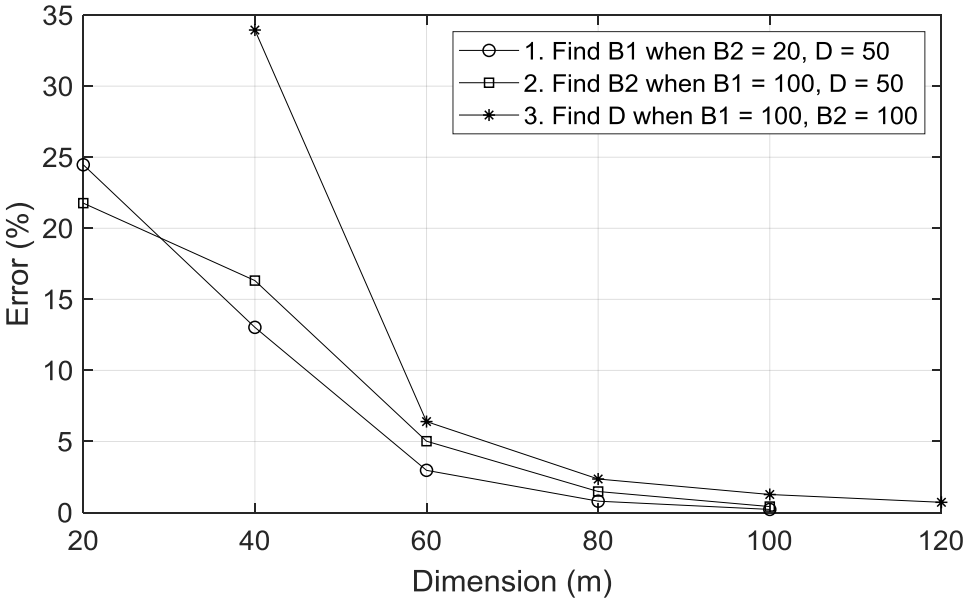

Fig. 6. Convergence study for finding optimal dimensions of the elastic half space.

The convergence study for the elastic half space was also carried out for various other combinations of B_1, B_2 and D as well (e.g. B_1 is calculated by fixing $B_2 = 100\,m$ and $D = 120\,m$). Although, the results are not presented here for brevity, the same results were observed.

4. Effect of soil anisotropy on exit gradient

Although the elastic half space is considered to be homogenous in the preliminary study discussed above, most of the soils are anisotropic in nature. Anisotropy depends upon the soil properties which defines the preferential flow direction in soils. Usually, in the compaction process, the soil is laid in horizontal layers and then compacted, therefore the tendency of flow is maximum in the horizontal direction. Anisotropy ratio relates the coefficient of permeability in different directions and is defined as the ratio of vertical to horizontal hydraulic conductivity (K_y/K_x). Anisotropy ratio of compacted soils typically varies between 0.025 to 1 [19]. Table 2 shows the effect of anisotropy on exit gradient. With the decrease in anisotropic ratio, the exit gradient increases. The analysis is carried out using 8-noded elements of an element size $h = 0.5\ m$.

Table 2. Convergence study for calculating the Depth of the soil domain.

K_y/K_x	Maximum Exit Gradient
0.025	0.5409
0.1	0.4965
0.25	0.4631
0.5	0.4295
1	0.3845
2	0.3285

5. Effect of scouring on exit gradient

The profile of a local scour is difficult to estimate due to the complexity of scour dynamics. Many experimental studies using laboratory tests have been performed in the past for predicting the depth, length, and shape of scour profile and its temporal growth. Oliveto *et al*. [20] investigated time-dependent and spatial evolution of local scour downstream below low-head spillways followed by stilling basins. Dehghani *et al*. [21] evaluated local scour characteristics downstream of rectangular sharp-crested weirs. In this paper, the geometry of the scour profile is chosen in accordance with the existing studies [20–22].

For the weir structure foundation with scouring, the convergence analysis is carried out for two different types of mesh refinement (a). Uniform mesh refinement (b). Adaptive mesh refinement (AMR). For simple geometries, a grid of uniform mesh spacing gives satisfactory results. However, for geometries that exhibit steep gradients or discontinuities, uniform mesh with very fine spacing can be used to minimize the estimated local error. But this approach can be computationally inefficient. Therefore, AMR is used in this study. In AMR approach, we start with a coarser mesh and identify the regions that needs finer mesh or the one with high mesh discretization error. Then, we superimpose finer mesh only on the identified regions. The process of superimposing finer mesh is done recursively until the measured error drops below some user defined value [23].

The scour starts at the toe of the stilling basin as shown in Fig. 7, where B_s is the width and D_s is the depth of the scour. In this analysis, homogenous soil layer with isotropic permeability is

considered and the scour profile is assumed to be $B_s = 5\,m$, $D_s = 2\,m$. The results of computational accuracy and convergence conducted for 4-noded, 6-noded, and 8-noded elements are presented in Table 3.

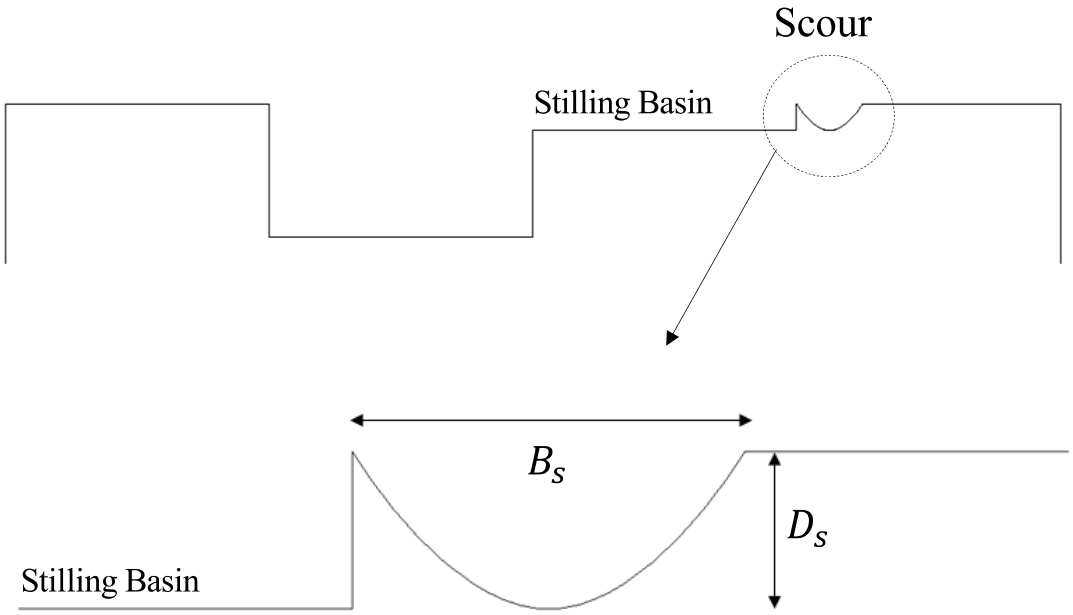

Fig. 7. Dimensions of the scour at the toe of the stilling basin.

For weir with a scour, based on optimal combination of efficiency and accuracy, 6-noded triangular element with adaptive meshing yield better results than 4-noded and 8-noded elements as the 6-noded triangular element is able to accurately represents the curved boundary profile of the scour.

Table 3. Results of convergence study for weir with scour.

$h\,(m)$	4-noded			6-noded			8-noded		
	i_{ex}	*Time*	*Error (%)*	i_{ex}	*Time*	*Error (%)*	i_{ex}	*Time*	*Error (%)*
2	0.4167	t		0.4764	t		0.5415	2t	
1	0.4993	3t	19.81	0.5529	2t	16.06	0.5632	3t	3.99
0.5	0.4950	10t	0.86	0.5541	7t	0.22	0.5488	17t	2.54
0.25	0.5218	42t	5.41	0.5532	28t	0.16	0.5517	47.2t	0.53
0.125	0.5366	225t	2.85	0.5542	138t	0.18	0.5538	253t	0.38
Adaptive	0.5462 (508t)			0.5545 (8t)			0.5538 (12t)		

The effect of downstream water depth on the maximum exit gradient in the scour profile is given in Table 4. As the downstream water level increases, the exit gradient decreases due to decrease in differential head in water levels between the upstream and the downstream sides of the weir structure.

The seepage analysis is also carrie d out for different scour profiles by varying the depth and the width of the scour. Table 5 shows the maximum exit gradient for different scour profiles. It is observed that the maximum exit gradient increases with increase in the scour depth and decrease in the scour width, which can lead to failure due to rupture much faster.

Table 4. Effect of Downstream water level on Maximum Exit Gradient.

Downstream water level, $H_{d/s}$ (m)	Maximum Exit Gradient
0	0.5545
0.5	0.5293
1	0.5041
1.5	0.4789
2	0.4537

Table 5. Maximum Exit Gradient for different scour profiles.

Scour width, $B_s(m)$	Scour depth, $D_s(m)$	Maximum Exit Gradient
2	0.5	0.5854
	1	0.8045
	1.5	1.0513
3	0.5	0.4836
	1	0.6228
	1.5	0.7508
	2	0.8513
4	1	0.5183
	1.5	0.5989
	2	0.6668
	2.5	0.7120
5	1	0.4596
	1.5	0.5116
	2	0.5545
	2.5	0.5868

6. Flooding fragility analysis

Flooding fragility curves are essential tools for assessing the vulnerability of a particular flood defense structure, and offer a means of communicating the probability of damage over a range of potential flooding levels. Fragility of a component or structure is defined as the conditional probability of failure, $P_{f|\lambda}$, to exceed a defined performance function, Z, at a given measure of intensity parameter λ e.g. flooding height. The performance function for this analysis is defined in section 2.3. The dimensions of the elastic half space: upstream width (B_1), the downstream width (B_2), and the depth (D) is taken as $120\ m$ for the fragility analysis. The fragility analysis is carried out using adaptive mesh refinement with 6-noded elements and is implement in ANSYS software [23] .

Fragilities are evaluated by considering uncertainties in variables that are used to characterize the local soil characteristics such as the anisotropic ratio, porosity, and specific gravity. The statistical distributions for the variables [8] incorporated in this study are shown in Fig. 8. A set of 250 random samples are generated from each of these normally distributed parameters. The analysis is carried out for such 250 random simulations with different heights of upstream water level ranging from 0 to 11 meters to calculate the probability of failure due to rupture. We have also studied the effect of number of samples on fragility analysis. We have divided all the samples into two equal parts: the first 125 samples and the last 125 samples. When we calculate

the failure probability for each part separately, there is not much variation in the failure probability. Therefore, 250 samples are sufficient, and we are not including the results in the manuscript for brevity. The fragility data is fitted to a cumulative lognormal distribution using maximum likelihood estimation.

Variation in fragility curves for different scour profiles by varying the scour width ($B_s = 2, 3, 4\ m$) with a fixed scour depth ($D_s = 1.5\ m$) and varying the scour depth ($D_s = 1, 1.5, 2\ m$) with a fixed scour width ($B_s = 3\ m$) are shown in Figs. 9 and 10 respectively.

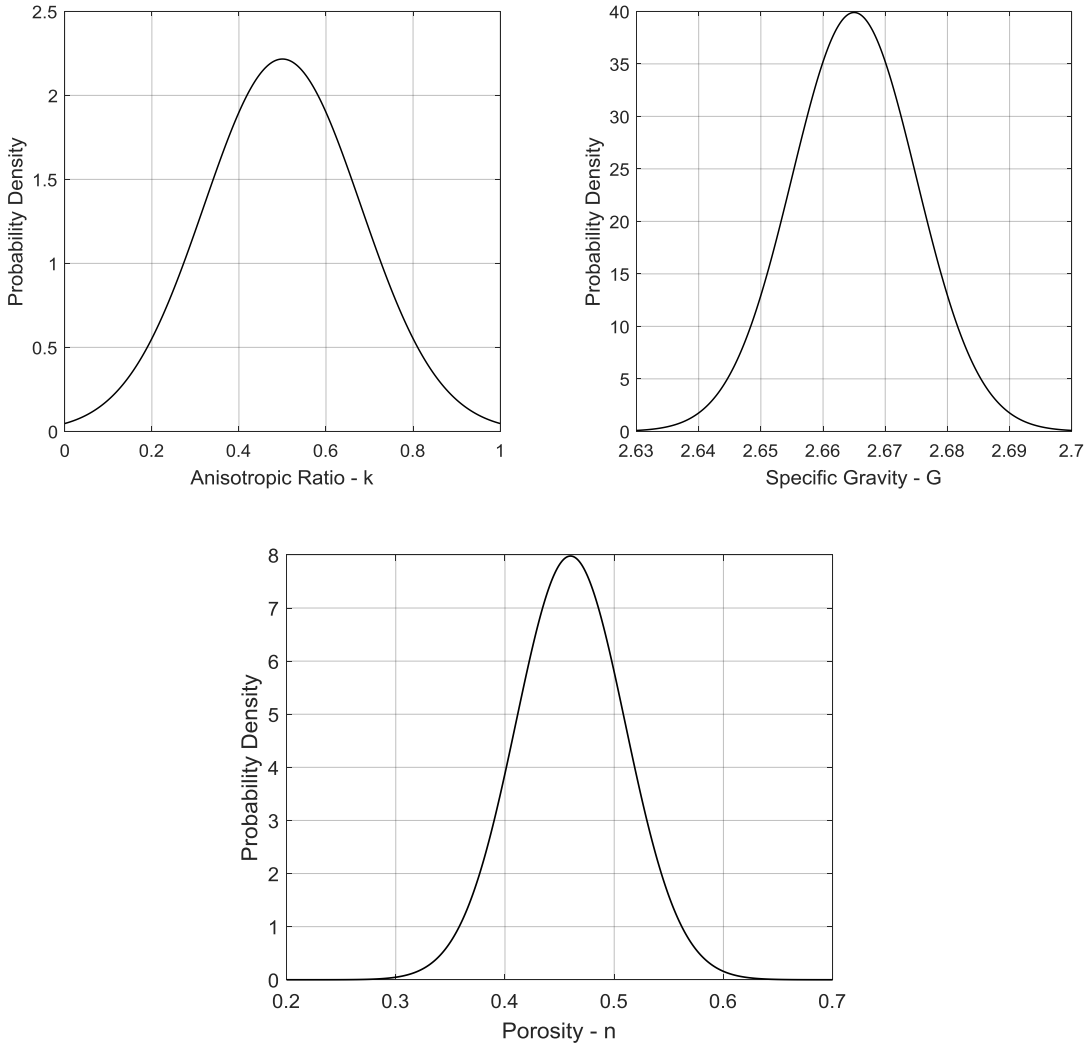

Fig. 8. Distributions of the random variables used to evaluate fragility curves.

The probability of failure due to rupture decreases with the increase in scour width for the same scour depth due to increase in distance between the toe of the stilling basin and the location of maximum scour depth. For scour profiles with fixed scour width, the rupture probability increases with increase in the scour depth.

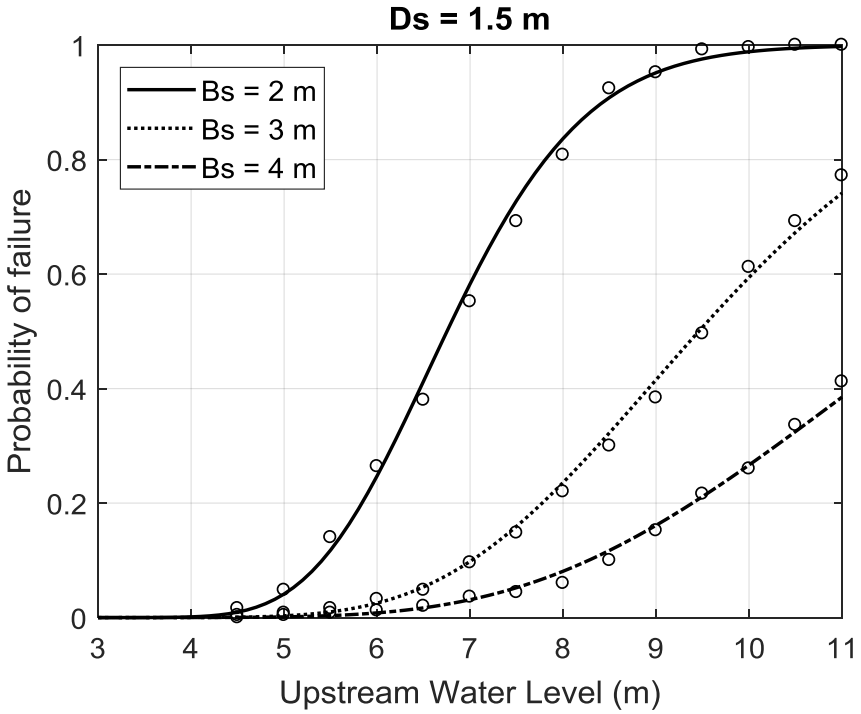

Fig. 9. Fragility curves for failure due to rupture for fixed $D_s = 1.5\ m$ and varying $B_s = 2, 3, 4\ m$.

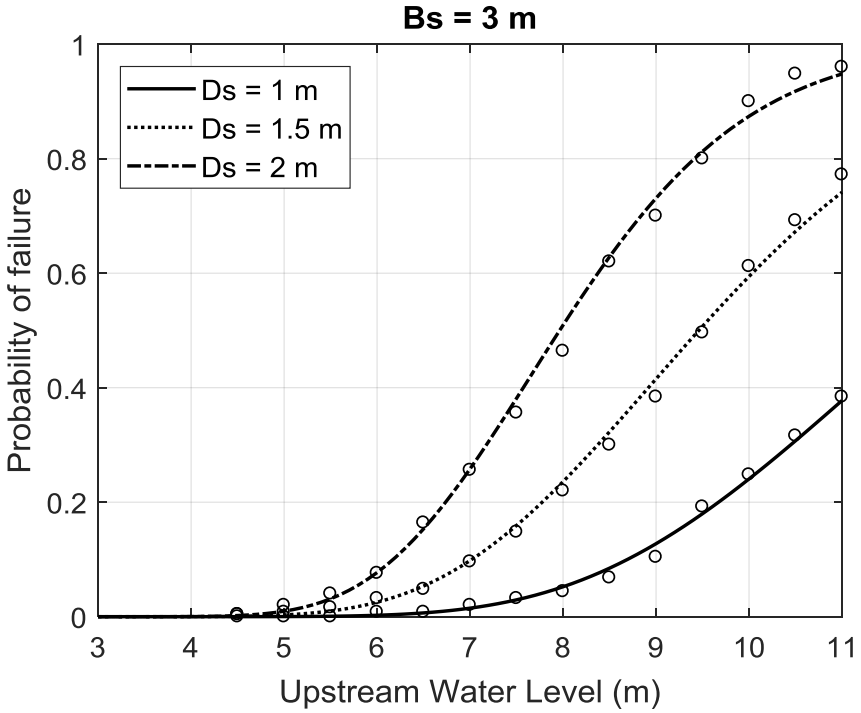

Fig. 10. Fragility curves for failure due to rupture for fixed $B_s = 3\ m$ and varying $D_s = 1, 1.5, 2\ m$

7. Conclusions

Uncontrolled seepage can lead to piping or undermining subsequently resulting in a failure due to rupture of the foundation. Local scour downstream of stilling basins can initiate the failure due to rupture much faster. The uncertainties in random variables influencing the failure due to rupture are incorporated and the rupture fragility curves for various scour profiles are obtained.

The key conclusions are:

- Advanced mesh techniques such as adaptive mesh refinement reduces the computational cost significantly.
- The anisotropic ratio (k_y/k_x) has a significant effect on the calculation of exit gradient. As the anisotropic ratio decreases, the exit gradient increases, thereby, the chances of failure due to rupture are increased.
- The proper location for the truncation boundary condition to represent the elastic half-space is investigated. According to the convergence analyses, the upstream width (B_1), the downstream width (B_2), and the depth (D) of the elastic half space should be at least 2.5 times more than the combined width of the weir structure and the stilling basin.
- For a constant upstream flood level, the probability of failure due to rupture decreases with the increase in scour width for the same scour depth. As the scour depth increases with time, the exit gradient increases with a consequent risk to failure of the structure.

References

[1] FEMA P-1090 / DR-4285-NC. Hurricane Matthew in North Carolina Dam Risk Management Assessment Report. 2017. n.d.

[2] Kayen R, Collins B, Gibbons H. USGS scientists investigate new Orleans levees broken by Hurricane Katrina. USGS Https://Soundwaves Usgs Gov/2006/01/ Accessed August 2006;15:2017.

[3] U.S. Army Corps of Engineers. Seepage Analysis and Control for Dams. EM 1110-2-1901; 1993 n.d.

[4] Billstein M, Svensson U, Johansson N. Development and Validation of a Numerical Model of Flow Through Embankment Dams–Comparisons with Experimental Data and Analytical Solutions. Transp Porous Media 1999;35:395–406.

[5] Khassaf SI, Al-Adili AS, Rasheed RS. Seepage analysis underneath Diyala weir foundation. Proc. Thirteen Int. Water Technol. Conf. IWTC, Hurghada, Egypt, Citeseer; 2009, p. 12–5.

[6] Olonade KA, Agbede OA. A study of seepage through oba dam using finite element method. Civ Environ Res 2013;3:53–60.

[7] Kirra MS, Zeidan BA, Shahien M, Elshemy M. Seepage Analysis of Walter F. George Dam, USA: A case Study. Int. Conf. Adv. Struct. Geotech. Eng., 2015, p. 1–13.

[8] Sandhu HK. Flooding Fragility of Concrete Gravity Dam-Foundation System 2015.

[9] Naouss WA, Najjar YM. Seepage design charts for flat bottom dams resting on heterogeneous media. Int J Numer Anal Methods Geomech 1995;19:637–51. doi:10.1002/nag.1610190904.

[10] Bardet J-P, Tobita T. A practical method for solving free-surface seepage problems. Comput Geotech 2002;29:451–75.

[11] Broaddus MR. Performing a steady-state seepage analysis using SEEP/W: a primer for engineering students. 2015.

[12] Elnikhely EA. Investigation and analysis of scour downstream of a spillway. Ain Shams Eng J 2018;9:2275–82. doi:10.1016/j.asej.2017.03.008.

[13] Ju BS, Jung W. Evaluation of seismic fragility of weir structures in South Korea. Math Probl Eng 2015;2015.

[14] Kratochvíl J, Bachorec T. Numerical Modeling of Nonstationary Free Surface Flow in Embankment Dams. Brno Univ Technol CZ 2004.

[15] Ahlinhan MF, Adjovi CE. Combined Geometric Hydraulic Criteria Approach for Piping and Internal Erosion in Cohesionless Soils. Geotech Test J 2018;42:20170096. doi:10.1520/GTJ20170096.

[16] S Ismaeel K, Noori BMA. Evaluation of seepage and stability of duhok dam. AL-Rafdain Eng J 2011;19:42–58.

[17] Soleymani S, Akhtarpur A. Seepage Analysis for Shurijeh Reservoir Dam Using Finite Element Method. Geo-Frontiers 2011, Reston, VA: American Society of Civil Engineers; 2011, p. 3227–34. doi:10.1061/41165(397)330.

[18] Hasani H, Mamizadeh J, Karimi H. Stability of slope and seepage analysis in earth fills dams using numerical models (Case Study: Ilam Dam-Iran). World Appl Sci J 2013;21:1398–402.

[19] Sommai L. Vertical and horizontal permeability of compacted soils. 1992 n.d.

[20] Oliveto G, Comuniello V. Local scour progress downstream of low-head stilling basins 2010.

[21] Dehghani AA, Bashiri H, Meshkati Shahmirzadi ME. Local scouring due to flow jet at downstream of rectangular sharp-crested weirs. WSEAS Int. Conf. Proceedings. Mech. Eng. Ser., vol. 5, World Scientific and Engineering Academy and Society; 2010.

[22] Farhoudi J, Shayan HK. Investigation on local scour downstream of adverse stilling basins. Ain Shams Eng J 2014;5:361–75. doi:10.1016/j.asej.2014.01.002.

[23] ANSYS (R16.2) Mechanical APDL Theory Reference n.d.